

Supporting information

A red thermally activated delayed fluorescence emitter with mitigated efficiency roll-off via π -stacked multiple donor-acceptor structure

Min Song,^{†ab} You-Jun Yu,^{†ab} Zi-Qi Feng,^{ab} Zhi-Hao Qu,^{ab} Peng Zuo,^{ab} Hong-Yan Yan,^{ab} Zuo-Quan Jiang,^{ab} Dong-Ying Zhou,^{*ab} Liang-Sheng Liao^{*abc}

^a *Institute of Functional Nano & Soft Materials (FUNSOM), Soochow University, Suzhou, 215123 Jiangsu, China.*

^b *Jiangsu Key Laboratory for Carbon-Based Functional Materials & Devices, Soochow University, Suzhou, 215123, Jiangsu, China.*

^c *Macao Institute of Materials Science and Engineering, Macau University of Science and Technology, Taipa, 999078 Macau, China.*

[†] Min Song and You-Jun Yu contributed equally to this work.

* E-mail: dyzhou@suda.edu.cn; lsiao@suda.edu.cn

Experimental section

General information

All chemicals and reagents were used as received from commercial resources without further purification. ^1H NMR and ^{13}C NMR spectra were measured on a Bruker 400 at room temperature. Mass spectra were performed on a Bruker Autoflex II.

Differential scanning calorimetry (DSC) was performed on a TA DSC 2010 unit at a heating rate of $10\text{ }^\circ\text{C}/\text{min}$ under nitrogen. The glass transition temperature (T_g) was determined from the second heating scan. Thermogravimetric analysis (TGA) was performed on TA SDT 2960 instrument at a heating rate of $10\text{ }^\circ\text{C}/\text{min}$ under nitrogen, the temperature at 5% weight loss was used as the decomposition temperature (T_d).

The electrochemical measurement was made using a CHI600 voltammetric analyzer. A conventional three-electrode configuration consisting of a platinum working electrode, a Pt-wire counter electrode, and an Ag/AgCl reference electrode was used. The solvent in the measurement was CH_2Cl_2 , and the supporting electrolyte was 0.1 M tetrabutylammonium hexafluorophosphate. Ferrocene was added as a calibrant after each set of measurements, and all potentials reported were quoted regarding the ferrocene-ferrocenium (Fc/Fc^+) couple at a scan rate of $100\text{ mV}/\text{s}$.

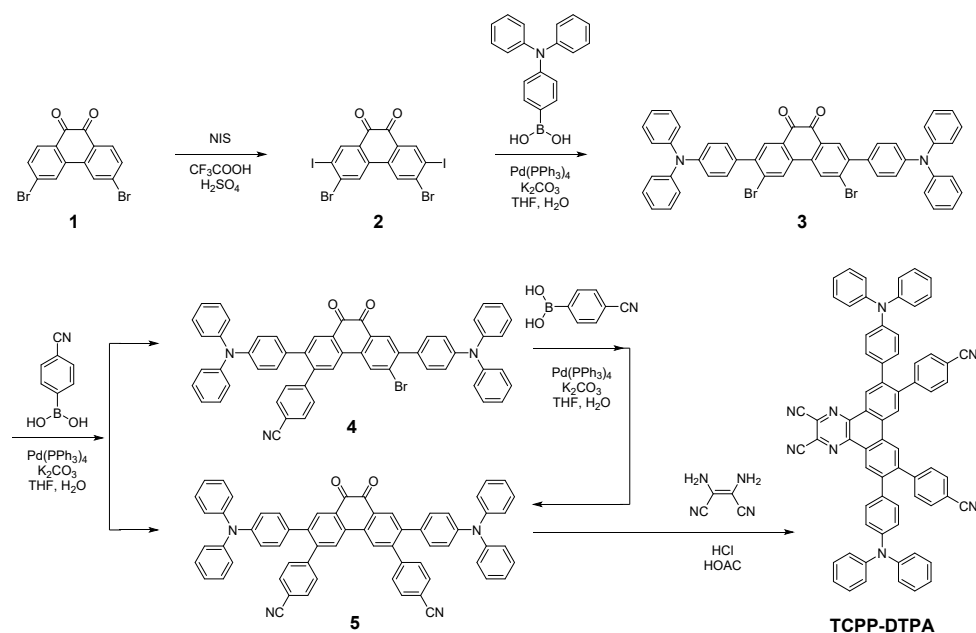
UV-vis absorption spectra were recorded on a Shimadzu UV 2600 spectrophotometer. Photoluminescence (PL) spectra and phosphorescent spectra were performed on Hitachi F-4600 fluorescence spectrophotometer and HORIBA FL-1000 fluorescence spectrophotometer. The absolute PLQY values were measured using Hamamatsu C9920-02G in an integrating sphere under a nitrogen atmosphere. The PLQY measurement range can cover from 300 nm to 950 nm. Transient spectra were obtained by using the Quantaaurus-Tau fluorescence lifetime measurement system (C11367-03, Hamamatsu Photonics Co.) in a vacuum.

Theoretical calculations based on density functional theory (DFT) and time-dependent density functional theory (TD-DFT) approach at the B3LYP/6-31G (d, p) level were performed with the use of the Gaussian 09 program.^[1] The topological properties were determined with the Multiwfn program.^[2]

Device fabrication and measurement

The OLEDs were fabricated by vacuum deposition technology. All the functional layers were fabricated on pretreated ITO substrates. The glass substrates coated with ITO layers were sequentially cleaned ultrasonically with acetone and ethanol, then dried in an oven at $110\text{ }^\circ\text{C}$ for 1 h. After being treated with ultraviolet-ozone plasma, the substrates were transferred into the evaporating chamber. OLED devices were fabricated through vacuum deposition under 4×10^{-6} Torr. After the deposition of functional layers, OLED device characterization was carried out at room temperature. EL spectra, luminance, and current density-voltage-luminance characteristics were measured under a constant source Keithley 2400 Source Meter and Photo Research PR 745 spectrophotometer.

Synthesis and characterization



Scheme S1. Synthetic routes for TCPP-DTPA

Compound 2 was synthesized according to the literature.¹

Synthesis of compound 3

Under nitrogen conditions, a mixture of compound 2 (1.00 g, 1.62 mmol), (4-(diphenylamino)phenyl)boronic acid (1.03 g, 3.56 mmol), Pd(PPh₃)₄ (0.19 g, 0.16 mmol), K₂CO₃ (1.34 g, 9.7 mmol) in 120 mL tetrahydrofuran and 30 mL degassed water was refluxed overnight. After cooling to room temperature, the reaction mixture was extracted with dichloromethane several times. The solvent was removed under reduced pressure, and then the residue was purified by column chromatography on silica gel using petroleum ether/dichloromethane (1/1, v/v) as the eluent, 0.9 g purple solid was finally obtained. Yield 65%. ¹H NMR (400 MHz, Chloroform-*d*) δ 8.26 (s, 2H), 8.14 (s, 2H), 7.35 – 7.27 (m, 12H), 7.19 – 7.15 (m, 8H), 7.14 – 7.10 (m, 4H), 7.10 – 7.06 (m, 4H). ¹³C NMR (101 MHz, Chloroform-*d*) δ 179.15, 148.24, 147.27, 144.04, 133.64, 132.80, 132.02, 131.73, 130.01, 129.98, 129.41, 129.19, 125.02, 123.54, 121.91. ESI-MS (*m/z*) of C₅₀H₃₂Br₂N₂O₂ for [M]⁺: calcd. 852.63; found, 852.76.

Synthesis of compound 4

Under nitrogen conditions, a mixture of compound 3 (1.00 g, 1.17 mmol), (4-cyanophenyl)boronic acid (0.41 g, 2.81 mmol), Pd(PPh₃)₄ (0.14 g, 0.12 mmol), K₂CO₃ (10.6 g, 76.7 mmol) in 150 mL tetrahydrofuran and 50 mL degassed water was refluxed overnight. After cooling to room temperature, the reaction mixture was extracted with dichloromethane several times. The solvent was removed under reduced pressure, and then the residue was purified by column chromatography on silica gel using petroleum ether/dichloromethane (2/3 to 1/4, v/v) as the eluent, 0.15 g dark green solid of compound 4 was finally obtained. Yield 15%. ¹H NMR (400 MHz, Chloroform-*d*) δ 8.33 – 8.29 (m, 2H),

8.19 (d, $J = 0.9$ Hz, 1H), 7.94 (s, 1H), 7.72 – 7.66 (m, 2H), 7.48 – 7.42 (m, 2H), 7.38 – 7.29 (m, 11H), 7.22 – 7.17 (m, 4H), 7.17 – 7.06 (m, 11H), 7.00 – 6.93 (m, 4H). ^{13}C NMR (101 MHz, Chloroform- d) δ 179.50, 179.43, 148.23, 147.83, 147.28, 147.13, 145.81, 144.92, 143.80, 142.21, 134.47, 133.02, 132.81, 132.70, 132.14, 132.05, 131.79, 131.05, 130.70, 130.32, 130.24, 130.01, 129.96, 129.42, 129.05, 126.25, 125.03, 124.96, 123.61, 123.55, 122.13, 121.94, 118.51, 111.81. ESI-MS (m/z) of $\text{C}_{57}\text{H}_{36}\text{BrN}_3\text{O}_2$ for $[\text{M}]^+$: calcd. 874.84; found, 874.38.

Synthesis of compound 5

Under nitrogen conditions, a mixture of compound 4 (1.00 g, 1.17 mmol), (4-cyanophenyl)boronic acid (0.34 g, 2.29 mmol), $\text{Pd}(\text{PPh}_3)_4$ (0.07 g, 0.06 mmol), K_2CO_3 (10.6 g, 76.7 mmol) in 150 mL tetrahydrofuran and 50 mL degassed water was refluxed overnight. After cooling to room temperature, the reaction mixture was extracted with dichloromethane several times. The solvent was removed under reduced pressure, and then the residue was purified by column chromatography on silica gel using petroleum ether/dichloromethane (1/4, v/v) as the eluent, 0.45 g purple solid of compound 5 was finally obtained. Yield 43%. ^1H NMR (400 MHz, Chloroform- d) δ 8.29 – 8.25 (m, 2H), 7.94 (s, 2H), 7.66 – 7.60 (m, 4H), 7.42 – 7.37 (m, 4H), 7.30 – 7.24 (m, 8H), 7.10 – 7.04 (m, 12H), 6.93 (s, 8H). ^{13}C NMR (101 MHz, Chloroform- d) δ 179.70, 147.78, 147.10, 145.83, 144.99, 141.93, 133.76, 132.57, 132.08, 131.03, 130.64, 130.30, 130.22, 129.42, 126.10, 124.95, 123.62, 122.07, 118.45, 111.75. ESI-MS (m/z) of $\text{C}_{64}\text{H}_{40}\text{N}_4\text{O}_2$ for $[\text{M}]^+$: calcd. 897.05; found, 897.32.

Synthesis of TCPP-DTPA

Under nitrogen conditions, a mixture of compound 5 (0.76 g, 0.85 mmol), 2,3-diaminomaleonitrile (0.11 g, 1.02 mmol) in 80 mL acetic acid was refluxed overnight. After cooling to room temperature, the reaction mixture was poured into water. The solid was filtered off, washed with water, and dried under a vacuum. The crude product was purified by column chromatography on silica gel using petroleum ether/dichloromethane (1/1, v/v) as the eluent, 0.50 g red solid was finally obtained. Yield 61%. ^1H NMR (400 MHz, Chloroform- d) δ 9.26 (s, 2H), 8.55 (s, 2H), 7.67 (d, $J = 8.0$ Hz, 4H), 7.49 (d, $J = 7.9$ Hz, 4H), 7.30 (t, $J = 7.7$ Hz, 8H), 7.19 – 6.95 (m, 20H). Due to poor solubility, ^{13}C NMR was not obtained. MALDI-TOF-MS (m/z) of $\text{C}_{64}\text{H}_{40}\text{N}_4\text{O}_2$ for $[\text{M}]^+$: calcd. 968.420; found, 968.420.

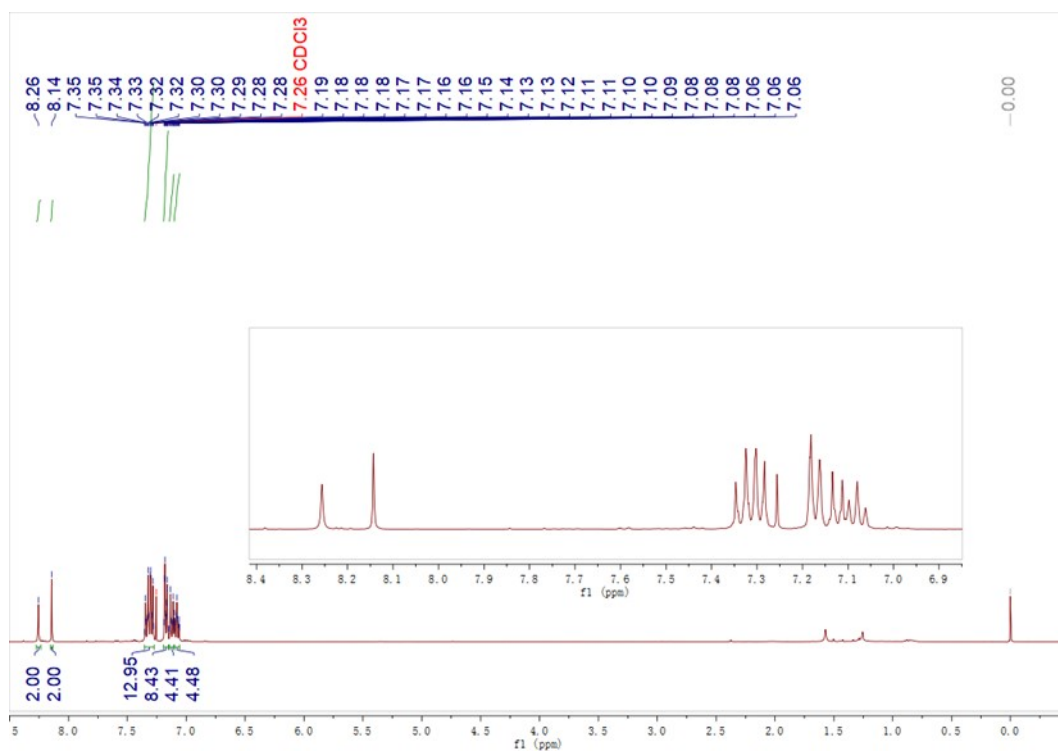


Figure S1. ¹H NMR (CDCl₃, 400 MHz) of compound 3

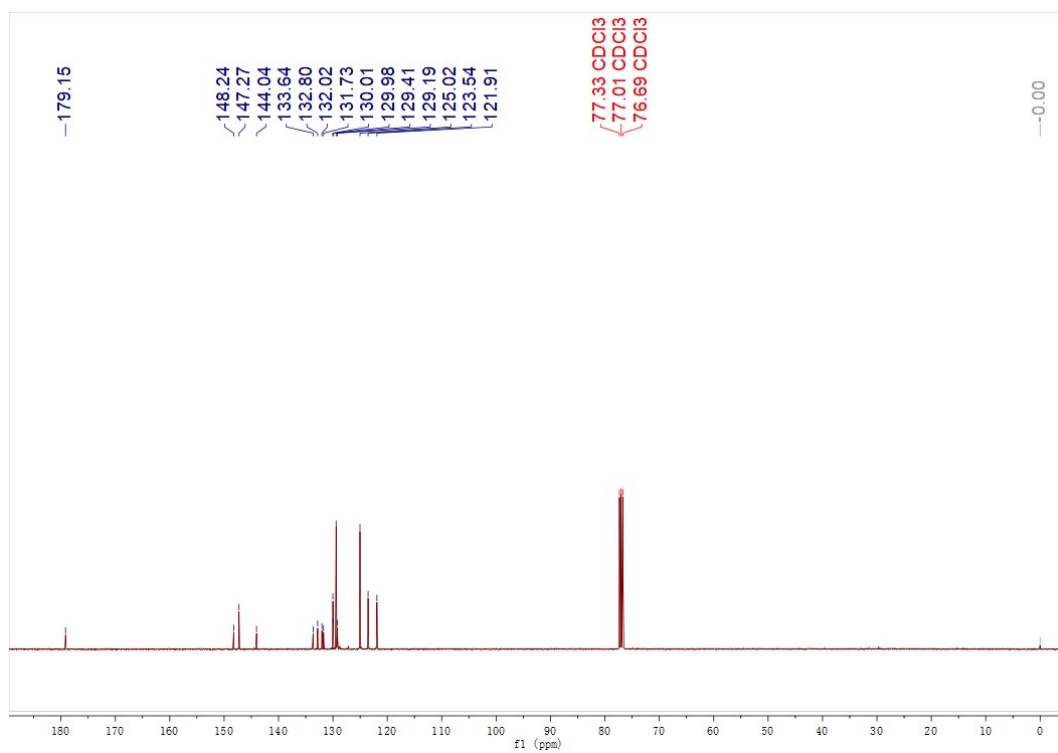


Figure S2. ¹³C NMR (CDCl₃, 101 MHz) of compound 3

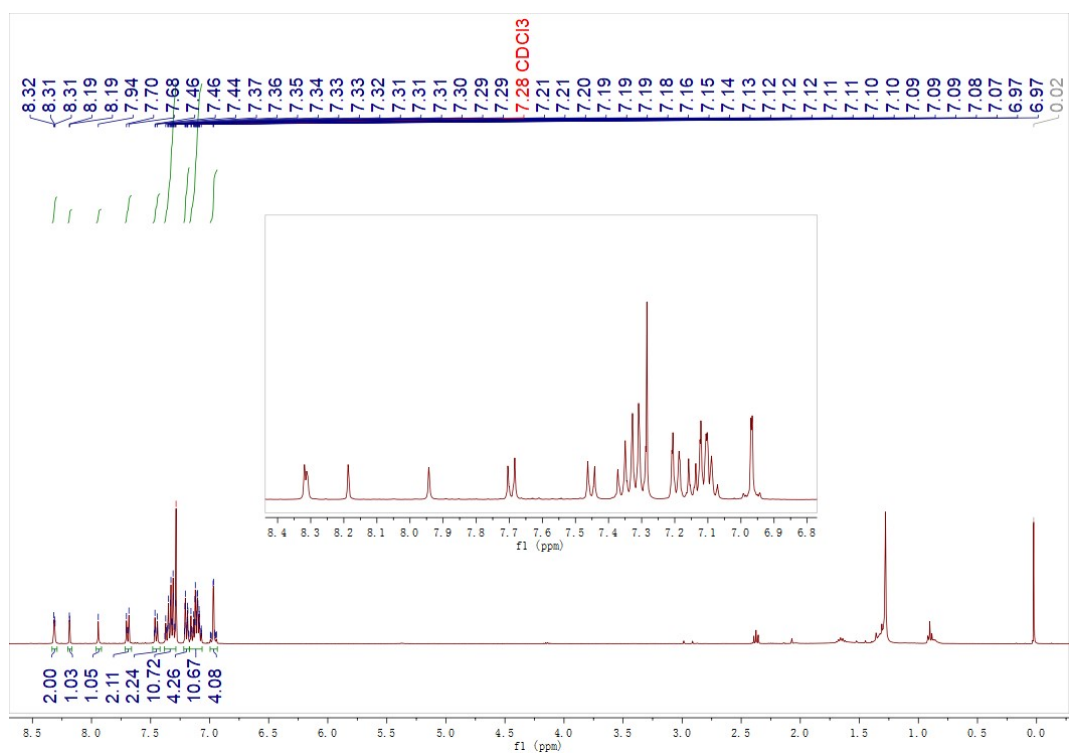


Figure S3. ^1H NMR (CDCl_3 , 400 MHz) of compound 4.

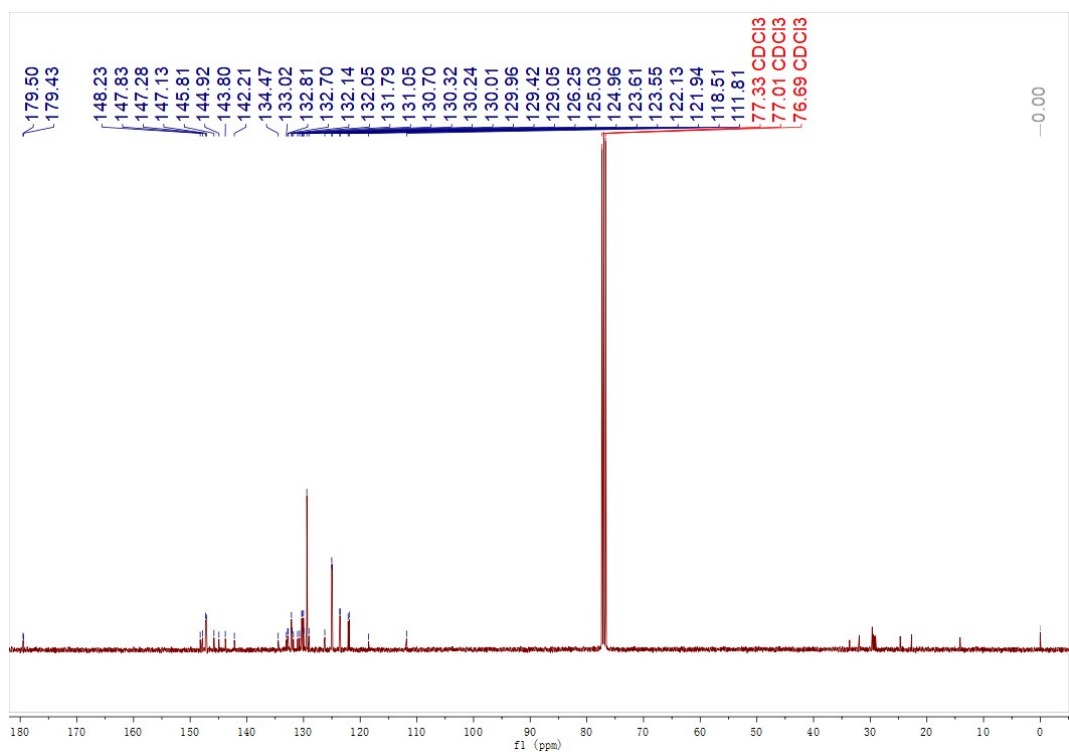


Figure S4. ^{13}C NMR of (CDCl_3 , 101 MHz) compound 4.

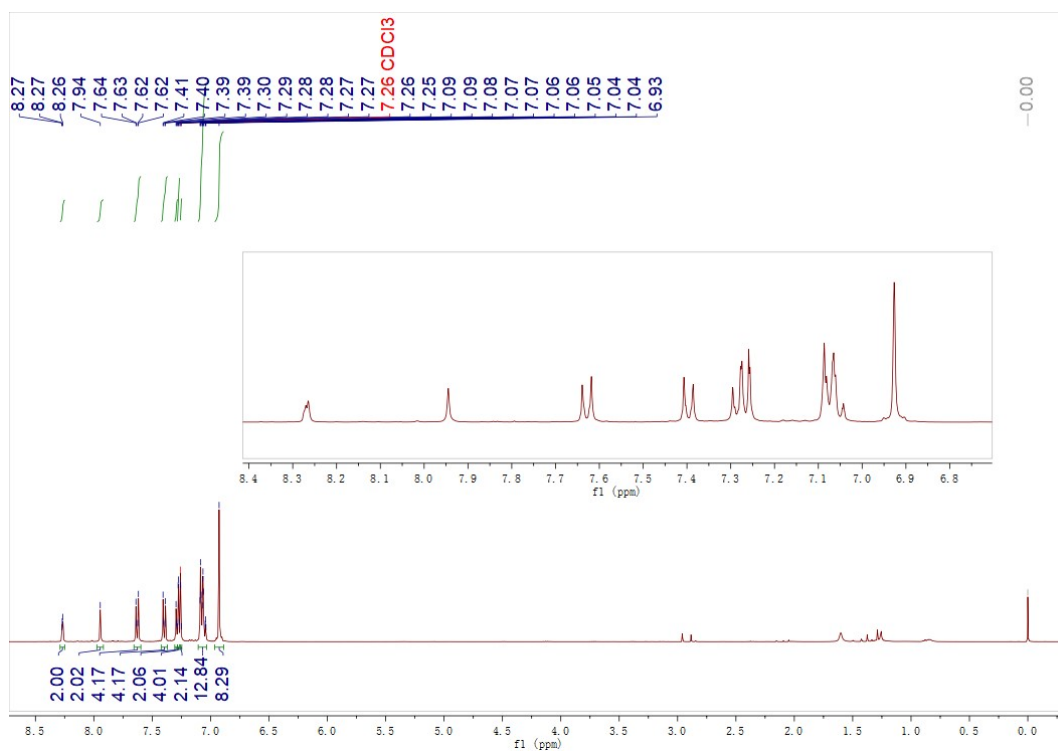


Figure S5. ¹H NMR (CDCl₃, 400 MHz) of compound 5.

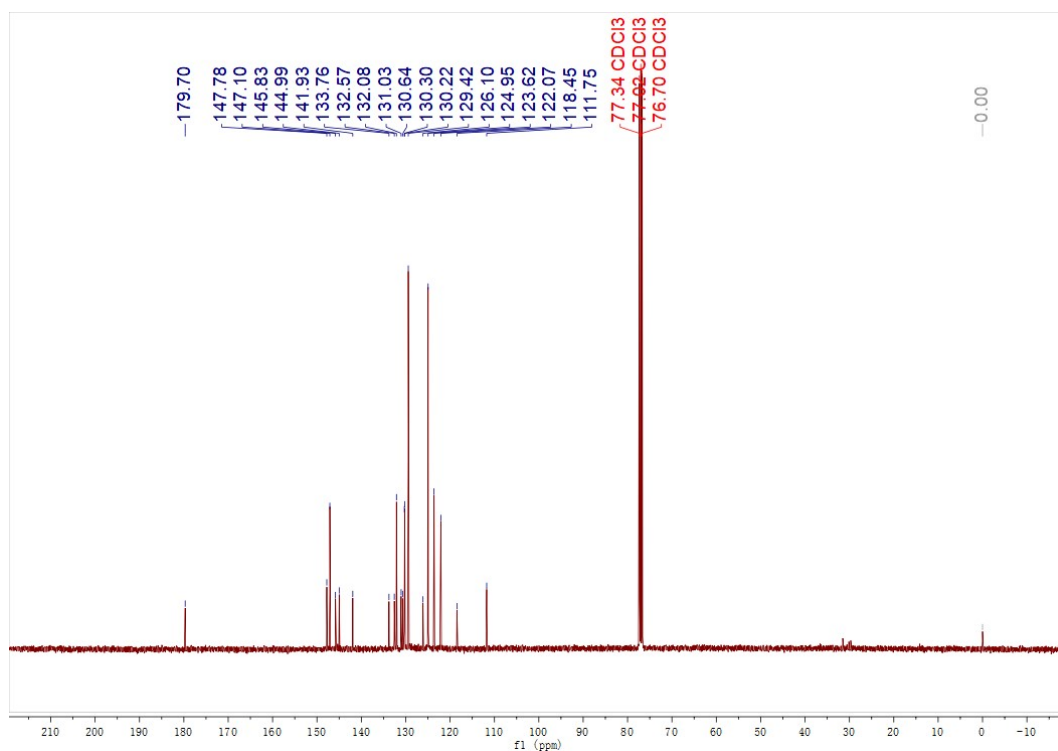


Figure S6. ¹³C NMR of (CDCl₃, 101 MHz) compound 5.

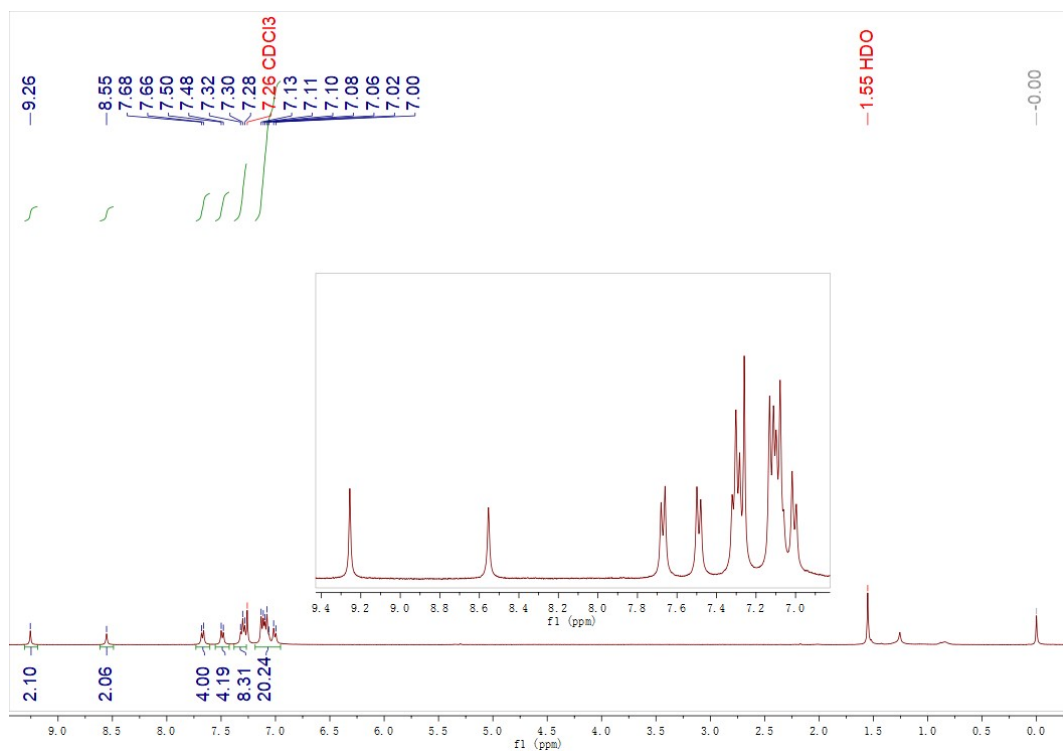


Figure S7. ¹H NMR (CDCl₃, 400 MHz) of TCPP-DTPA.

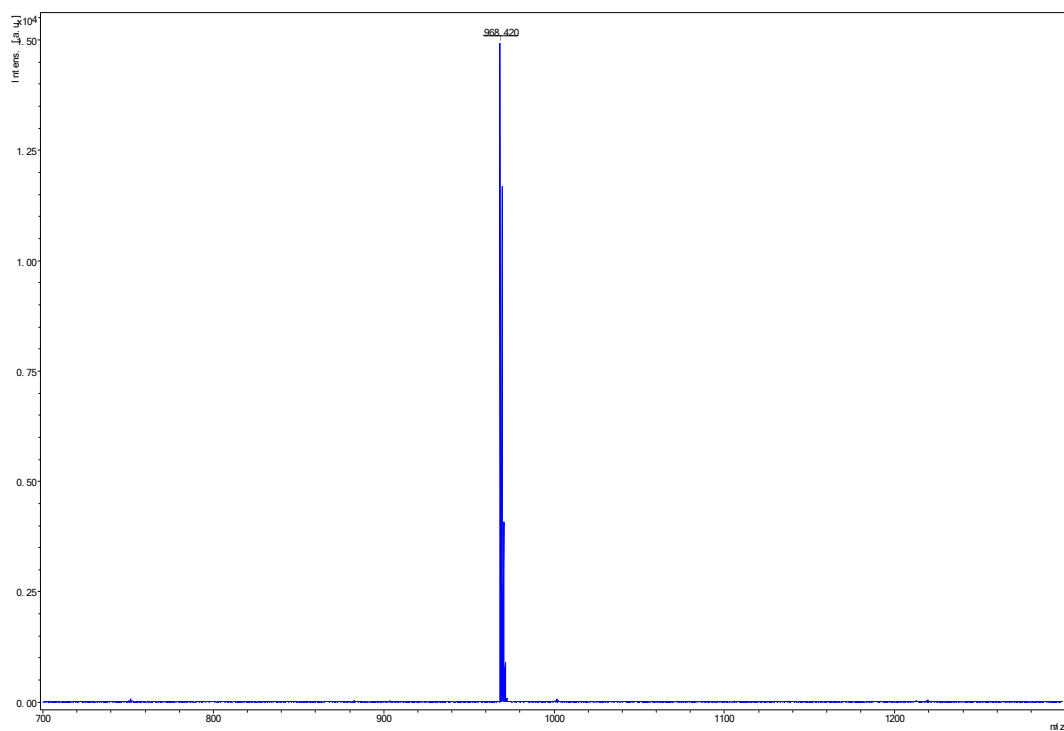


Figure S8. TOF-MS of TCPP-DTPA.

Thermal properties

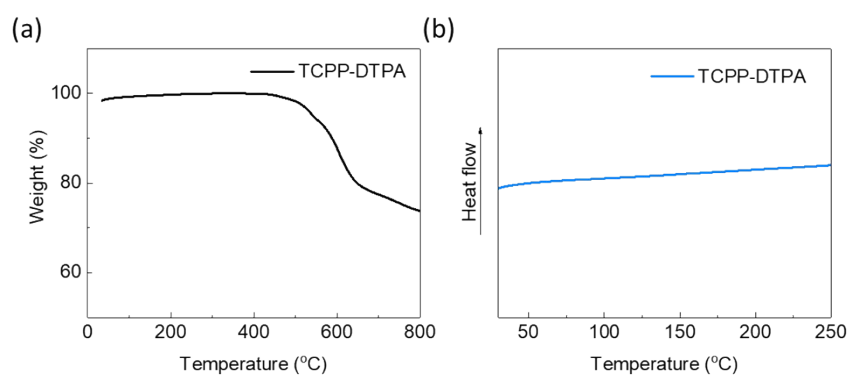


Figure S9. TGA (a) and DSC (b) curves of TCPP-DTPA.

Electrochemical properties

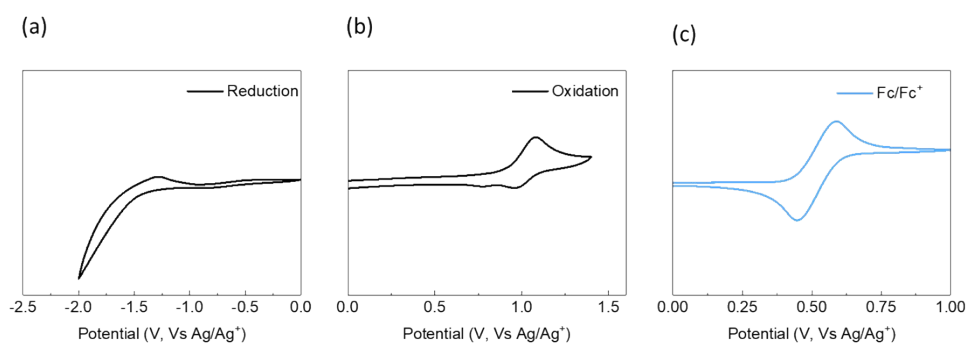


Figure S10. CV curves of (a) (b) TCPP-DTPA and (c) ferrocene.

Photochemical properties

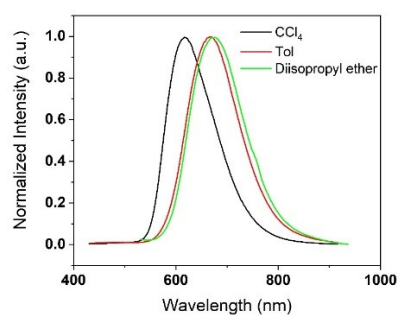


Figure S11. Fluorescence spectra of TCPP-DTPA in different solvents.

Single crystal

Table S1. Crystal data and structure refinement for TCPP-DTPA.

Identification code	TCPP-DTPA
Empirical formula	C ₇₀ H ₄₆ N ₈ O
Formula weight	1015.15
Temperature/K	100
Crystal system	triclinic
Space group	P-1
a/Å	12.906(9)
b/Å	14.638(7)
c/Å	16.846(8)
α/°	102.70(2)
β/°	99.20(3)
γ/°	116.118(19)
Volume/Å ³	2665(3)
Z	2
ρ _{calc} /cm ³	1.265
μ/mm ⁻¹	0.077
F(000)	1060.0
Crystal size/mm ³	0.12 × 0.08 × 0.05
Radiation	MoKα (λ = 0.71073)
2θ range for data collection/°	3.828 to 52.944
Index ranges	-15 ≤ h ≤ 16, -18 ≤ k ≤ 17, -17 ≤ l ≤ 21
Reflections collected	26474
Independent reflections	10834 [R _{int} = 0.0541, R _{sigma} = 0.0791]
Data/restraints/parameters	10834/0/714
Goodness-of-fit on F ²	1.012
Final R indexes [I ≥ 2σ (I)]	R ₁ = 0.0638, wR ₂ = 0.1793
Final R indexes [all data]	R ₁ = 0.1273, wR ₂ = 0.2195
Largest diff. peak/hole / e Å ⁻³	0.18/-0.21

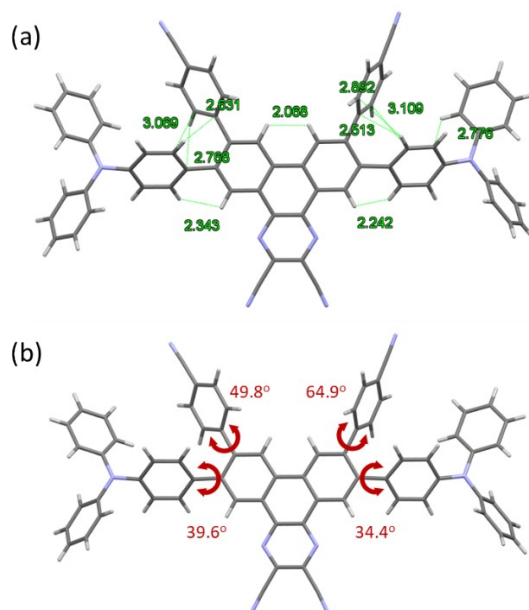


Figure S12. (a) intramolecular interactions and (b) dihedral angles of TCPP-DTPA.

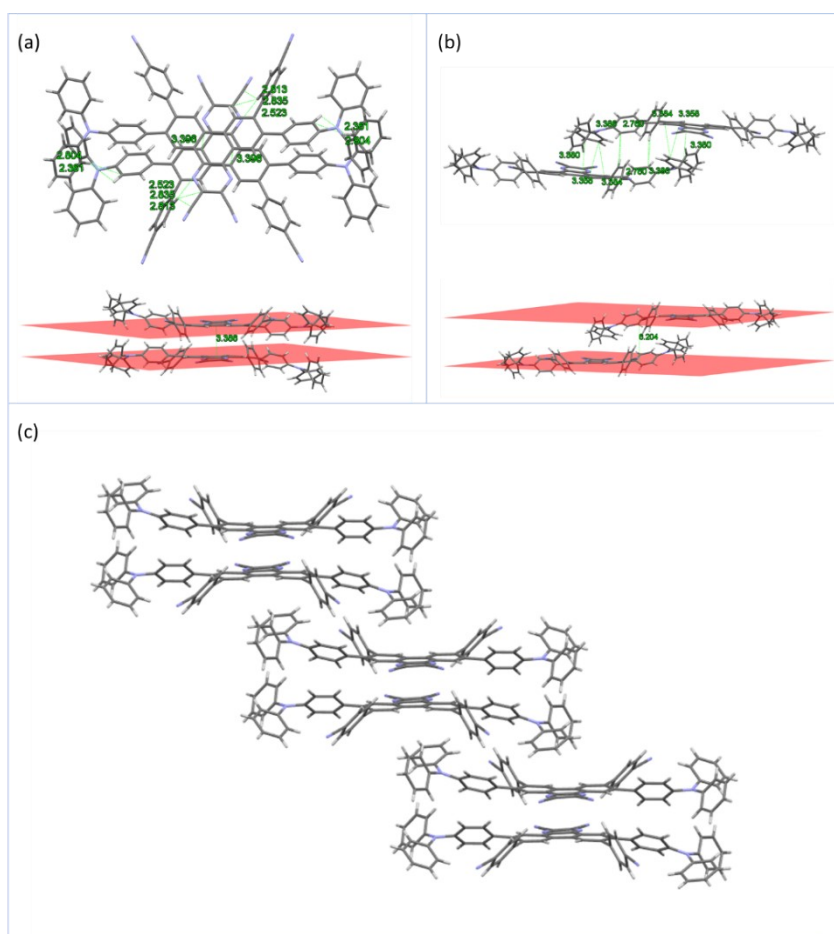


Figure S13. Intermolecular interactions and distances for (a) H-dimer (b) J-dimer and (c) packing modes.

Simulation results

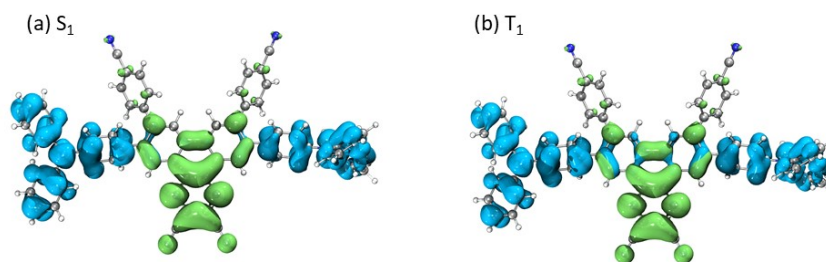


Figure S14. Hole (blue) and electron (green) distribution of S_1 and T_1 states for TCPP-DTPA.

Table S2. Simulation results of TCPP-DTPA.

Sample	HOMO [eV]	LUMO [eV]	E_g [eV]	E_{S1} [eV]	E_{T1} [eV]	ΔE_{ST} [eV]
TCPP-DTPA	-5.22	-3.06	2.16	1.81	1.76	0.05

Photophysical properties

Table S3. The summary of computing transient characterization in doped films.

Sample	τ_P (ns)	τ_D (μ s)	Φ_{total} (%)	Φ_{prompt} (%)	Φ_{TADF} (%)	k_P (s^{-1})	k_{ISC} (s^{-1})	k_r^s (s^{-1})	k_{nr}^s (s^{-1})	k_{RISC} (s^{-1})
TCPP-DTPA	50	5.9	95.4	3.5	91.9	2×10^7	1.48×10^7	6.92×10^5	3.34×10^4	4.67×10^6

In this work, the doped films of TCPP-DTPA do not exhibit phosphorescence emission at 300 K. In other words, the efficiency of phosphorescence is zero ($\Phi_{Phos} = 0$). Thus, the quantum efficiency of delayed emission (Φ_{DE}) is equal to the efficiency of delayed fluorescence (Φ_{DF}). Thus, the quantum efficiencies of prompt (Φ_{PF}) and delayed emission (Φ_{DF}) are evaluated by the corrected estimation method and the rate constants were calculated according to the reported method².

$$k_p = \frac{1}{\tau_{PF}}$$

$$k_d = \frac{1}{\tau_{DF}}$$

$$k_r^s = k_p \phi_{PF}$$

$$k_{nr}^s = k_p \frac{\phi_{PF}}{\phi_{all}} (1 - \phi_{all})$$

$$k_{ISC} = k_p \frac{\phi_{PF}}{\phi_{all}} - k_d \frac{\phi_{DF}}{\phi_{PF}}$$

$$k_{RISC} = k_d \frac{\phi_{all}}{\phi_{PF}}$$

$$k_{nr}^T = 0$$

Where k_p and k_d are the radiative decay rate for prompt and delayed fluorescence, respectively; ϕ_{all} is the total photoluminescence quantum efficiency; k_r^s and k_{nr}^s are the radiative and nonradiative decay rate constants from a singlet excited state, respectively; k_{ISC} and k_{RISC} are the intersystem crossing and reverse intersystem crossing rate constants, respectively; k_{nr}^T is the nonradiative decay rate constant from a triplet excited state

Electroluminescent properties

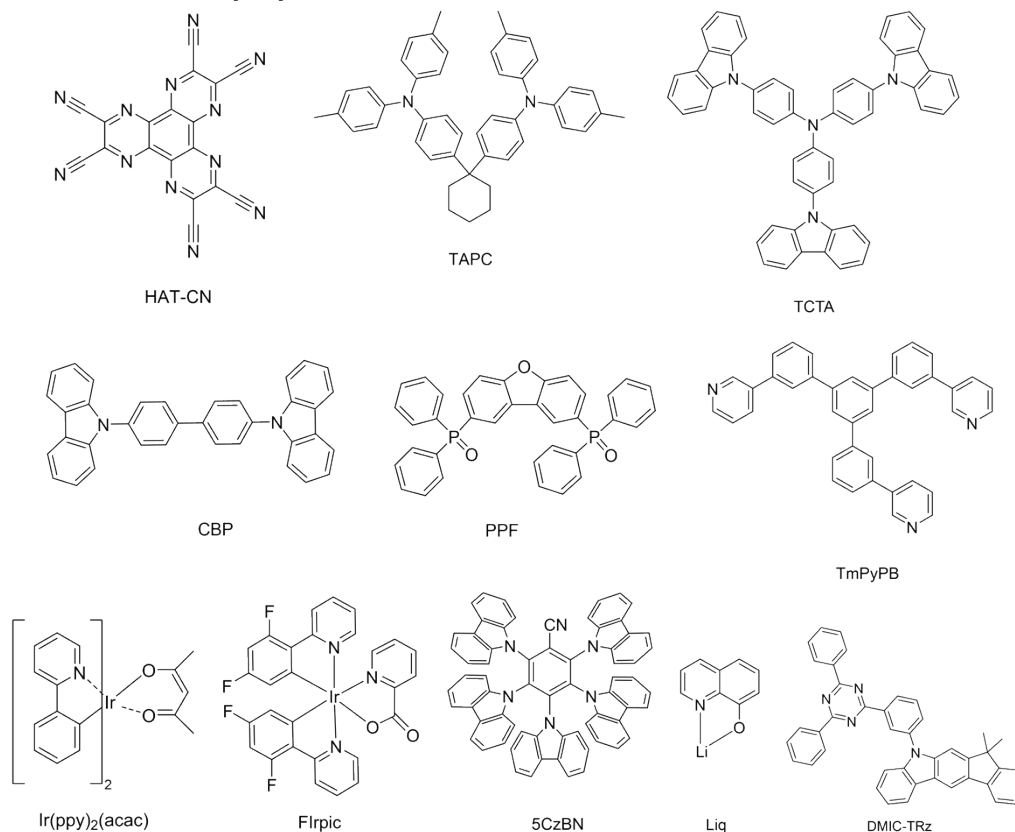


Figure S15. Molecular structures for HAT-CN, TAPC, TCTA, CBP, PPF, TmPyPB, $\text{Ir}(\text{ppy})_2(\text{acac})$, Flrpic, Liq, DMIC-TRz, and 5CzBN.

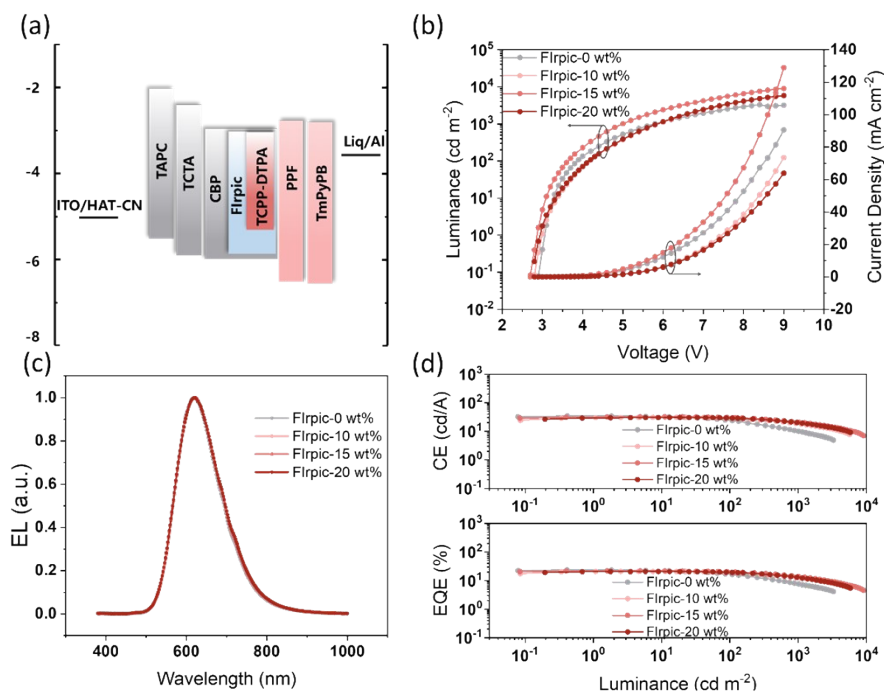


Figure S16. Device performance of the sensitized device with varying doping ratios of Flrpic as an assistant dopant. (a) The electronic energy level diagram; (b) J-V-L curves; (c) EL spectra; (d) CE-L and EQE-L curves.

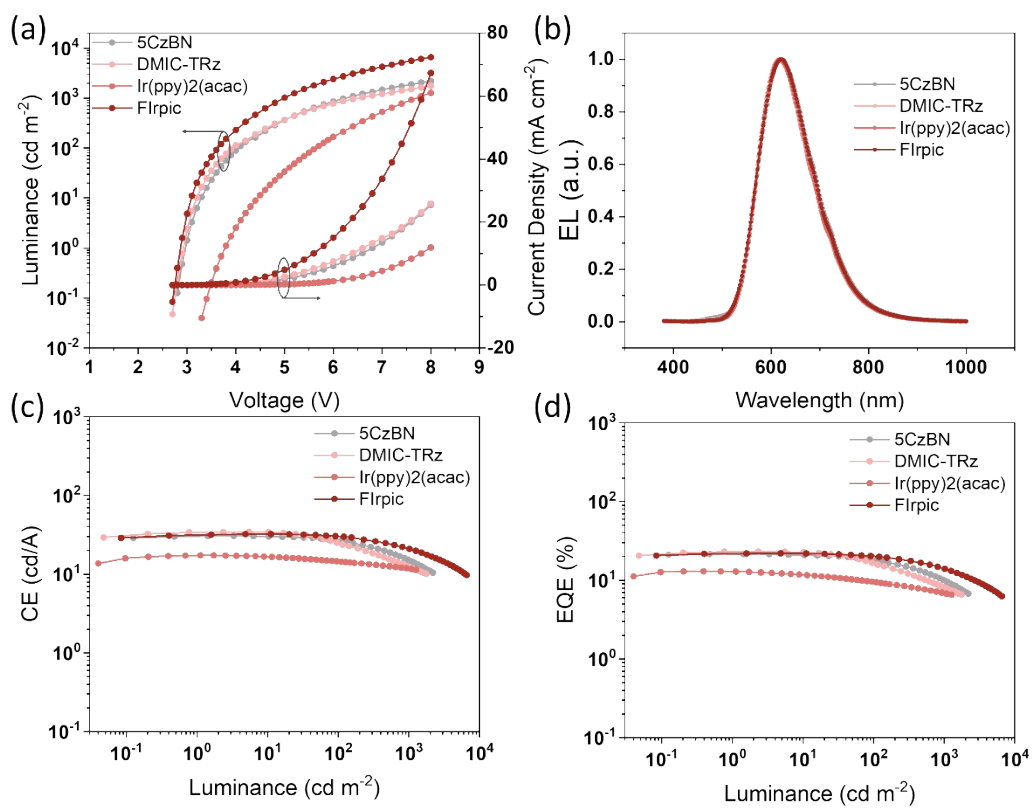


Figure S17. The J–V–L (a), EL spectra (b), CE–L (c), and EQE–L (d) characteristics of devices with different assistant dopants.

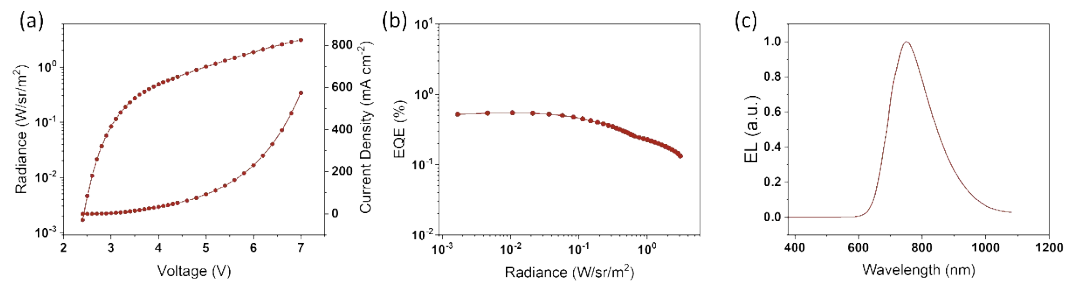


Figure S18. The J–V–R (a), EQE–R (b), EL spectra (c) characteristics of non-doped OLED with 100% TCPP-DTPA.

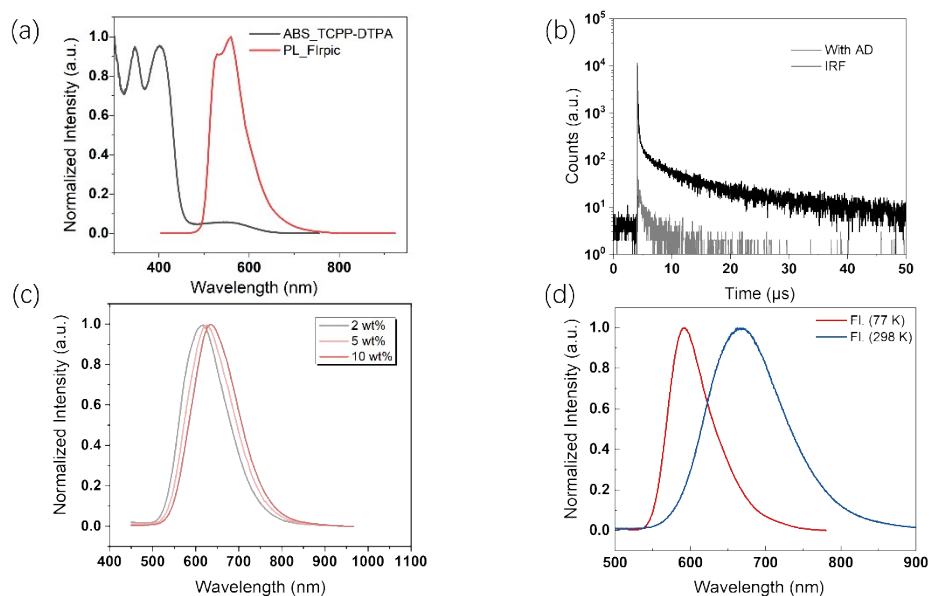


Figure S19. (a) Absorption spectrum of TCPP-DTPA in dilute toluene (10^{-5} M) and the photoluminescence spectrum of FIrpic film (15 wt% in CBP); (b) Time-resolved photoluminescence spectrum of 2 wt% TCPP-DTPA with AD doped in the CBP film. (c) Fluorescence spectra of different ratios of TCPP-DTPA in the doped CBP films. (d) PL spectra of TCPP-DTPA in low-temperature (77 K) and room-temperature (298 K) toluene.

Table S4. The PLQY and fluorescence emission peaks of different doping ratios TCPP-DTPA doped in CBP films.

Doping ratio	2 wt%	5 wt%	10 wt%
PLQY [%]	95.4	83.3	68.9
λ [nm]	613	624	634

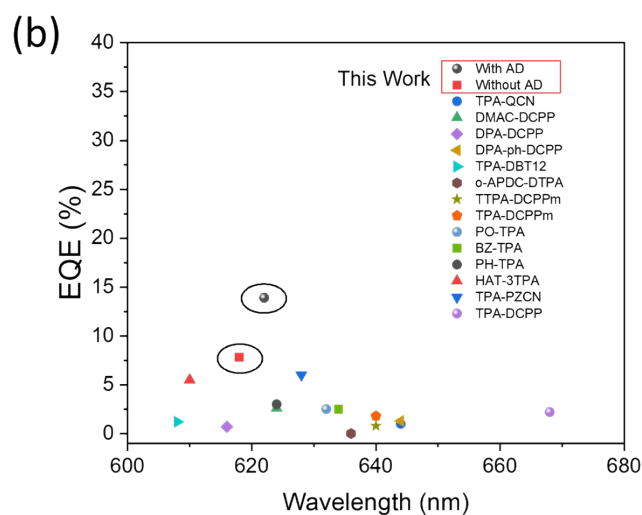
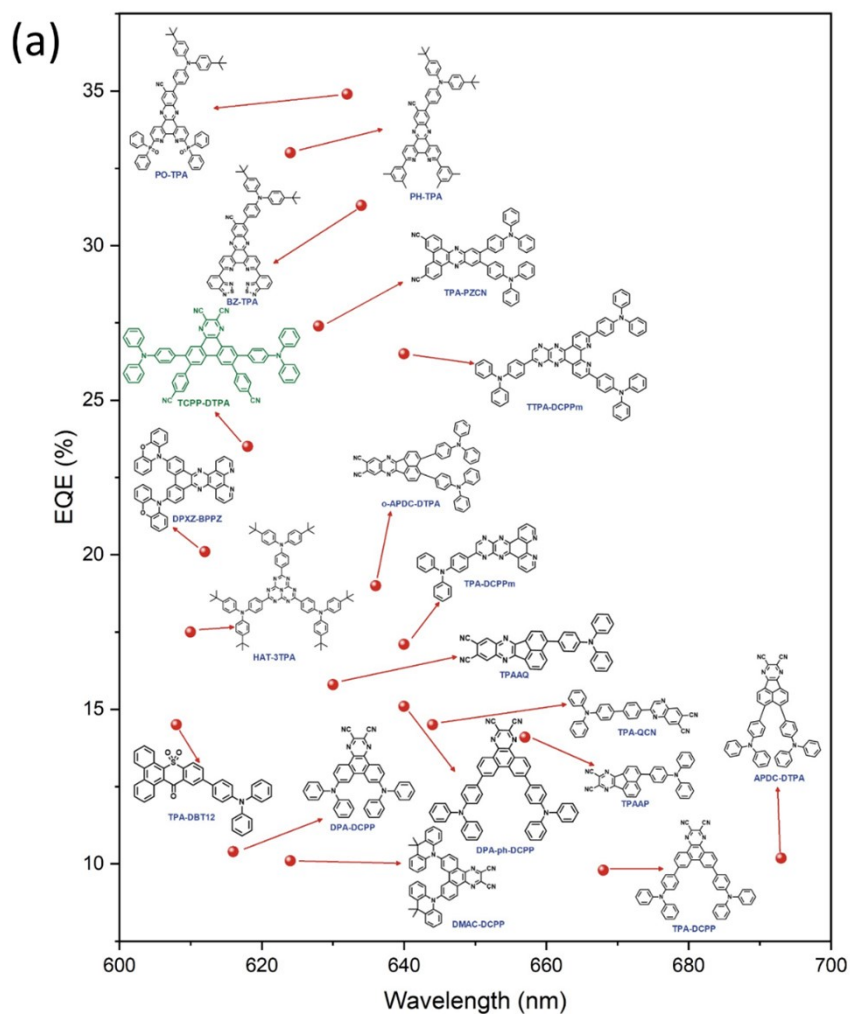


Figure S20. (a) Molecular structure of organic red TADF emitters plotted as EQE_{max} versus EL peak wavelength; (b) Statistics of EQE at 1000 cd m^{-2} values with these emitters.

Table S5. EQE_{max} and EQE at 1000 cd m⁻² of OLED devices with different red TADF emitters.

Emitter	EQE _{max}	EQE@1000 cd m ⁻²	λ _{EL} [nm]
T CPP-DTPA	23.5	7.83/14.9	618
TPA-QCN ³	14.5	1	644
TPAAP ⁴	14.1	-	657
TPAAQ ⁴	15.8	-	630
DMAC-DCPP ⁵	10.1	2.6	624
DPA-DCPP ⁵	10.4	0.7	616
TPA-DBT ¹²	14.5	1.2	608
DPA-ph-DCPP ⁵	15.1	1.3	640
o-APDC-DTPA ⁷	19	0.01	636
TTPA-DCPPm ⁸	26.5	0.8	640
TPA-DCPPm ⁸	17.1	1.8	640
PO-TPA ⁹	34.9	2.5	632
BZ-TPA ⁹	31.3	2.5	634
PH-TPA ⁹	33	3	624
HAT-3TPA ¹⁰	17.5	5.5	610
TPA-PZCN ¹¹	27.4	6	628
APDC-DTPA ¹²	10.19	-	693
DPXZ-BPPZ ¹³	20.1	-	612
TPA-DCPP ¹⁴	9.8	2.2	668

References

1. Kumar, N.; Nielsen, K. E.; Maiti, S.; Petersen, M., Triplex Formation with α-L-LNA (α-L-Ribo-Configured Locked Nucleic Acid). *J. Am. Chem. Soc.* **2006**, *128* (1), 14-15.
2. Tsuchiya, Y.; Diesing, S.; Bencheikh, F.; Wada, Y.; Dos Santos, P. L.; Kaji, H.; Zysman-Colman, E.; Samuel, I. D. W.; Adachi, C., Exact Solution of Kinetic Analysis for Thermally Activated Delayed Fluorescence Materials. *J. Phys. Chem. A.* **2021**, *125* (36), 8074-8089.
3. Li, C.; Duan, R.; Liang, B.; Han, G.; Wang, S.; Ye, K.; Liu, Y.; Yi, Y.; Wang, Y., Deep-Red to Near-Infrared Thermally Activated Delayed Fluorescence in Organic Solid Films and Electroluminescent Devices. *Angew. Chem. Int. Ed. Engl.* **2017**, *56* (38), 11525-11529.
4. Xue, J.; Liang, Q.; Wang, R.; Hou, J.; Li, W.; Peng, Q.; Shuai, Z.; Qiao, J., Highly Efficient Thermally Activated Delayed Fluorescence via J-Aggregates with Strong Intermolecular Charge Transfer. *Adv. Mater.* **2019**, *31* (28), e1808242.
5. Wang, S.; Cheng, Z.; Song, X.; Yan, X.; Ye, K.; Liu, Y.; Yang, G.; Wang, Y., Highly Efficient Long-Wavelength Thermally Activated Delayed Fluorescence OLEDs Based on Dicyanopyrazino Phenanthrene Derivatives. *ACS Appl. Mater. Interfaces* **2017**, *9* (11), 9892-9901.
6. Hu, X.; Qin, Y.; Li, Z.; Gao, H.; Gao, T.; Liu, G.; Dong, X.; Tian, N.; Gu, X.; Lee, C.-S.; Wang, P.; Wang, Y., Nearly 100% exciton utilization in highly efficient red OLEDs based on dibenzothioxanthone

acceptor. *Chinese Chem. Lett.* **2022**, *33* (10), 4645-4648.

7. Wang, H.; Wang, J.; Zou, P.; Xu, J.; Li, J.; Shi, H.; Zhao, Z.; Tang, B. Z., Efficient thermally activated delayed fluorescence emitters with regioisomeric effects for red/near-infrared organic light-emitting diodes. *Mater. Chem. Front.* **2023**, *7* (8), 1633-1641.
8. Yang, H.-Y.; Zhang, H.-Y.; Zhang, M.; Zhuo, H.; Wang, H.; Lin, H.; Tao, S.-L.; Zheng, C.-J.; Zhang, X.-H., Simultaneously optimizing radiative decay and up-conversion of triphenylamine-based thermally activated delayed fluorescence emitters to achieve efficient deep-red organic light-emitting diodes. *Chem. Eng. J.* **2023**, *468*, 143721 .
9. Liang, J.-X.; Pan, Z.-H.; Zhang, K.; Yang, D.; Tai, J.-W.; Wang, C.-K.; Fung, M.-K.; Ma, D.; Fan, J., A facile method to achieve red thermally activated delayed fluorescence emitters with EQE over 30% via molecular aspect ratio engineering. *Chem. Eng. J.* **2023**, *457*, 141074.
10. Li, J.; Nakagawa, T.; MacDonald, J.; Zhang, Q.; Nomura, H.; Miyazaki, H.; Adachi, C., Highly efficient organic light-emitting diode based on a hidden thermally activated delayed fluorescence channel in a heptazine derivative. *Adv. Mater.* **2013**, *25* (24), 3319-3323.
11. Zhang, Y. L.; Ran, Q.; Wang, Q.; Liu, Y.; Hanisch, C.; Reineke, S.; Fan, J.; Liao, L. S., High-Efficiency Red Organic Light-Emitting Diodes with External Quantum Efficiency Close to 30% Based on a Novel Thermally Activated Delayed Fluorescence Emitter. *Adv. Mater.* **2019**, *31* (42), e1902368.
12. Yuan, Y.; Hu, Y.; Zhang, Y. X.; Lin, J. D.; Wang, Y. K.; Jiang, Z. Q.; Liao, L. S.; Lee, S. T., Over 10% EQE Near - Infrared Electroluminescence Based on a Thermally Activated Delayed Fluorescence Emitter. *Adv. Funct. Mater.* **2017**, *27* (26), 1700986.
13. Chen, J. X.; Wang, K.; Zheng, C. J.; Zhang, M.; Shi, Y. Z.; Tao, S. L.; Lin, H.; Liu, W.; Tao, W. W.; Ou, X. M.; Zhang, X. H., Red Organic Light-Emitting Diode with External Quantum Efficiency beyond 20% Based on a Novel Thermally Activated Delayed Fluorescence Emitter. *Adv. Sci.* **2018**, *5* (9), 1800436.
14. Wang, S.; Yan, X.; Cheng, Z.; Zhang, H.; Liu, Y.; Wang, Y., Highly Efficient Near-Infrared Delayed Fluorescence Organic Light Emitting Diodes Using a Phenanthrene-Based Charge-Transfer Compound. *Angew. Chem. Int. Ed. Engl.* **2015**, *54* (44), 13068-13072.